Kinetics and Products of the IO + BrO Reaction

David M. Rowley,† William J. Bloss,‡ R. Anthony Cox,* and Roderic L. Jones

Centre for Atmospheric Science, University Chemical Laboratories, University of Cambridge, Lensfield Road, Cambridge, CB2 1EW, U.K.

Received: December 14, 2000; In Final Form: April 12, 2001

The kinetics and products of reaction 1 between gas-phase BrO and IO radicals have been studied using the technique of laser photolysis with time-resolved UV−vis absorption spectroscopy. The O + IBr reaction 8, used as one source of IO and BrO radicals, was found to produce predominantly IO radicals at 295 K. The rate coefficient for reaction 8 is correlated with the branching ratio for IO production (channel 8a). Using a value of 0.7 for the branching ratio for IO production (k_{8a}/k_8), k_8 was found to be $(3.6 \pm 2.4) \times 10^{-11}$ cm^3 molecule^{-1} s^{-1} at 295 K, with no significant temperature dependence between 210 and 333 K. Sensitivity tests using a kinetic model showed that, in addition to (1), decay traces were also sensitive to the rate coefficient for reaction 12: I + BrO → Br + IO. This rate coefficient was found to be $(1.3 \pm 1.2) \times 10^{-11}$ molecule^{-1} cm^3 s^{-1} at 295 K, with no significant temperature dependence between 235 and 333 K. The title reaction (1), IO + BrO → products was found to have a rate coefficient $(8.5 \pm 1.4) \times 10^{-11}$cm^3 molecule^{-1} s^{-1} at 295 K. Reaction 1 exhibited a negative temperature dependence between 210 and 333 K, adequately described by $k_1 = (6.7 \pm 0.8) \times 10^{-12} \exp((760 \pm 30)/T)$ molecules^{-1} cm^3 s^{-1}. No pressure dependence to k_1 was found between 100 and 760 Torr. All errors are 2σ. Five potential products exist for the IO + BrO reaction: IO + BrO → I + Br + O_2 (1a), IO + BrO → IBr + O_2 (1b), IO + BrO → OIO + Br (1c), IO + BrO → OBrO + I (1d), and IO + BrO → $IBrO_2$ (1e). No direct measurement of I or Br formation was perfomed. IBr was observed as a minor product ($k_{1b}/k_1 < 0.2$). OIO formation was observed and shown to result from the IO + BrO reaction for the first time in this work. No evidence for OBrO formation was observed ($k_{1d}/k_1 < 0.15$). No evidence for the formation or existence of $IBrO_2$ was observed. The results obtained here, in conjunction with other published work, were used to constrain the branching ratio, α, for OIO production in the IO + IO reaction, giving $\{0.30 \pm 0.05 \leq \alpha \leq 0.46 \pm 0.08\}$. This constraint allowed the absorption cross section of OIO to be constrained giving $(1.29 \pm 0.22) \geq \sigma_{OIO} \times 10^{17} \geq 0.87 \pm 0.15)$ molecules^{-1} cm^2 at the (5,1,0) peak at 549 nm, 295 K, and 760 Torr. Results are compared with previous studies of the IO + BrO reaction, and the atmospheric implications are briefly discussed.

1. Introduction

Gas-phase halogen monoxide free radicals can participate in reaction cycles which destroy atmospheric ozone. The origins and role of iodine containing species have been discussed in the accompanying paper[1] in which a study of the IO + IO reaction is described. In this paper, the coupling between iodine and bromine chemistry is considered in a study of the IO + BrO reaction.

In the low stratosphere, typical BrO abundances of over 10 of parts per trillion (pptv) are routinely observed.[2,3] In contrast, measurements aimed at detecting stratospheric IO initially reported an upper limit of 0.2 pptv for the IO abundance[4,5] although a recently reported measurement has indicated stratospheric IO abundances in the range 0.65−0.80 pptv.[6] At such concentrations the IO self-reaction makes a negligible contribution to ozone depletion; however, coupling between iodine species and members of other chemical families can lead to significant iodine-catalyzed ozone loss. The IO + BrO reaction is one such potential coupling reaction. Since the stratospheric abundance of BrO radicals is in general higher than that of IO radicals,[7] the IO + BrO reaction may occur significantly even at low IO concentrations; consequently, if the IO + BrO reaction produces I or Br atoms, ozone loss can occur even if IO concentrations are too low for the IO self-reaction to proceed rapidly.

The potential for very low concentrations of total iodine to destroy ozone in the stratosphere was originally described by Solomon et al.[8] In a modeling study, these authors found that 1 pptv of total iodine in the low stratosphere would be partitioned primarily into active (ozone destroying) forms I and IO. Moreover, Solomon et al. showed that, at a level of 1 pptv, iodine catalyzed ozone loss would dominate halogen catalyzed ozone loss in the low stratosphere. In carrying out this modeling study, Solomon et al. assumed that the IO + XO (X = Cl, Br) reactions both proceeded with rate coefficients of 1×10^{-10} molecule^{-1} cm^3 s^{-1}, and produced solely I + X + O_2 products. Occurrence of the IO + BrO reaction would thus lead to ozone loss via

$$\mathrm{IO + BrO \rightarrow I + Br + O_2} \quad (1a)$$

$$\mathrm{I + O_3 \rightarrow IO + O_2} \quad (2)$$

$$\mathrm{Br + O_3 \rightarrow BrO + O_2} \quad (3)$$

$$\mathrm{Net} \quad \mathrm{2O_3 \rightarrow 3O_2}$$

* To whom correspondence should be addressed. E-mail: rac26@cam.ac.uk. FAX: + 44 1223 336362.

† Present address: Jet Propulsion Laboratory, California Institute of Technology, Pasadena, CA 91109. E-mail: wbloss@jpl.nasa.gov.

‡ Present address: University College London, Chemistry Department, Christopher Ingold Laboratories, 20 Gordon Street, London WC1H 0AJ, UK. E-mail: d.m.rowley@ucl.ac.uk.

10.1021/jp004494y CCC: $20.00
Published on Web 07/27/2001

TABLE 1: Enthalpies of Formation of IO + BrO Reaction Moieties

species	$\Delta_f H°$ (298K)/kJ mol^{-1}	ref
IO	116 ± 5	41
BrO	120 ± 6	38
I	107	
Br	112	42
IBr	40.9	
OIO	76.7	17
OBrO	150	18

The IO + BrO reaction may also be of significance in the troposphere. IO and BrO radicals have both been observed in the marine boundary layer[9,10] and, while no simultaneous observation of IO and BrO has been reported, precursors to both species, such as the photolabile iodobromocarbon CH_2IBr, have been observed in the marine boundary layer.[11] The observation of elevated BrO concentrations correlates with reduced ozone concentrations in the marine boundary layer.[12] This can be explained in part by the occurrence of the relatively slow BrO + BrO reaction 4a; however, reaction 1a could also contribute to the observed ozone loss, even with low IO abundances, if k_{1a} were significantly greater than k_{4a}.

$$\mathrm{BrO} + \mathrm{BrO} \rightarrow 2\,\mathrm{Br} + \mathrm{O_2} \qquad (4a)$$

$$(k_{4a,295K} = 2.49 \times 10^{-12}\ \mathrm{molecule^{-1}\,cm^3\,s^{-1}}\ \text{(ref 13)})$$

By analogy with other halogen monoxide self- and cross-reactions,[14] five potential channels can be envisaged for the IO + BrO reaction:

$$\mathrm{IO} + \mathrm{BrO} \rightarrow \mathrm{I} + \mathrm{Br} + \mathrm{O_2} \qquad (1a)$$

$$\rightarrow \mathrm{IBr} + \mathrm{O_2} \qquad (1b)$$

$$\rightarrow \mathrm{OIO} + \mathrm{Br} \qquad (1c)$$

$$\rightarrow \mathrm{OBrO} + \mathrm{I} \qquad (1d)$$

$$\mathrm{IO} + \mathrm{BrO} + \mathrm{M} \rightarrow \mathrm{IBrO_2} + \mathrm{M} \qquad (1e)$$

The potential for the IO + BrO reaction to affect atmospheric ozone levels depends critically upon the reaction products: Occurrence of reaction channels 1a or 1b followed by IBr photolysis, will lead to catalytic ozone destruction, via reactions 2 and 3. The potential impact of channels 1c and 1d on ozone depends on the fate of the OXO species (X = I, Br) produced: if OXO photolyses to form O(^{3}P) + XO, in a manner analogous to OClO,[15] then channels 1c and 1d will lead to a null cycle with respect to atmospheric ozone loss. Conversely, if OXO is photostable, as has been argued for OIO,[16] some ozone loss is expected from the halogen atom coproduced in 1c and 1d, and the role of the IO + BrO reaction will depend on the subsequent fate of the OXO species. Similarly, the atmospheric implications of formation of $IBrO_2$ would depend on the structure and photochemical properties of this species. Thermodynamic data (Table 1) indicates that reactions 1a and 1b are exothermic, by 17 and 195 kJ mol^{-1}, respectively. Calculated values for the enthalpies of formation of OIO[17] and OBrO[18] indicate that channel (1c) is exothermic by 47 kJ mol^{-1}, while channel 1d is endothermic by 21 kJ mol^{-1}. The thermodynamic properties of the hypothesized $IBrO_2$ molecule are unknown.

The IO + BrO reaction has been the subject of three previous laboratory studies. Laszlo et al.[19] measured the overall rate coefficient at 298 K and 760 Torr using the flash photolysis/UV absorption technique, and found $k_1 = (6.9 \pm 2.7) \times 10^{-11}$ molecules^{-1} cm^3 s^{-1}. Subsequently, Gilles et al.[20] investigated the temperature dependence of reaction 1, using pulsed laser photolysis within a discharge flow system to generate the reactants, coupled with LIF detection of IO and UV absorption detection of BrO. Gilles et al. monitored the loss of IO radicals in the presence of excess O_3, and thus obtained the rate coefficient for the non-I atom producing channels of reaction 1, as channels producing an I atom led to IO regeneration via reaction 2 and were therefore effectively suppressed:

Gilles et al. obtained a value of $(6.05 \pm 0.57) \times 10^{-11}$ molecules^{-1} cm^3 s^{-1} for $(k_{1b} + k_{1c} + k_{1e})$ at 298 K and total pressures in the range 7−15 Torr. This result, in conjunction with the measurement of k_1 reported by Laszlo et al., indicates that non-I atom producing channels dominate the IO + BrO reaction at 298 K. Gilles et al. also found that non-I atom channels exhibited a negative temperature dependence, $(k_{1b} + k_{1c} + k_{1e})$ increasing to $(8.82 \pm 0.50) \times 10^{-11}$ molecules^{-1} cm^3 s^{-1} at 204 K. Bedjanian et al.[21] measured the overall rate coefficient k_1 and placed limits on branching ratios for the IO + BrO reaction at 298 K and 1 Torr total pressure, using the discharge flow/mass spectrometry technique. These authors report $k_1 = 8.5 \times 10^{-11}$ molecules^{-1} cm^3 s^{-1}, and that I atom producing channels have a combined branching ratio $((k_{1a} + k_{1d})/k_1) < 0.3$. Bedjanian et al. also report that OIO production dominated the IO + BrO reaction, with a branching ratio of $0.65 \le k_{1c}/k_1 \le 1$.

Two of the potential products of reaction 1 have recently been observed in the atmosphere. Tentative observations of atmospheric OIO have recently been reported.[22] However, our laboratory studies have shown that OIO is a product of the IO self-reaction[1] and measurements of atmospheric IO at the several pptv level which accompanied the OIO observations indicate that this reaction could be the source of the observed OIO. Measurements of OBrO in the nighttime stratosphere at concentrations of up to 20 pptv have also been reported,[23] although very recent measurements do not confirm these observations.[24] In the laboratory, OBrO formation has been observed and attributed to the reaction between between BrO and O_3,[13,25] and also as a product of the self-reaction of vibrationally excited BrO.[26] However, none of the currently understood bromine chemistry can explain the presence of significant amounts (>0.01 pptv) of OBrO in the stratosphere.[27]

Assessment of the atmospheric significance of the IO + BrO reaction throughout the atmosphere, and in particular the potential for iodine chemistry to contribute to stratospheric ozone loss, requires both the rate coefficient and branching ratio of reaction 1 to be established under appropriate conditions. In this paper, we report an investigation of the kinetics and products of the IO + BrO reaction as a function of temperature between 210 and 333 K, and as a function of pressure between 100 and 760 Torr.

2. Experimental Details

The IO + BrO reaction was studied using the technique of laser flash photolysis with kinetic UV absorption spectroscopy, utilizing a CCD detection system. The apparatus has been described in detail elsewhere[13,28] and briefly in the accompanying paper;[1] no further details are given here.

Radical Generation. Three chemical systems were employed to generate IO and BrO radicals, using different precursor gas mixtures: $I_2/Br_2/N_2O/N_2$, $IBr/N_2O/N_2$, and $CF_3I/Br_2/N_2O/N_2$, referred to hereafter as systems A, B, and C, respectively. Reaction initiation was achieved via 193 nm laser photolysis of N_2O to form O(^{1}D) + N_2, followed by rapid collisional quenching of the excited oxygen atoms to O(^{3}P). IO and BrO

TABLE 2: Precursor Concentration Ranges

system[a]	$N_2O \times 10^{-16}$	$I_2 \times 10^{-14}$	$Br_2 \times 10^{-15}$	IBr $\times 10^{-14}$	$CF_3I \times 10^{-16}$
A	0.57−9.9	1.4−4.8	2.0−15		
B	9.8			2.5−24	
C	9.8		7.9−19		3.7−8.7

[a] See text for details. Concentrations in molecules cm^{-3}. N_2 added to 1 atm total pressure.

radicals were generated by reaction of the $O(^3P)$ atoms with the halogen species:

$$N_2O + h\nu \rightarrow O(^1D) + N_2 \quad (5)$$

$$O(^1D) + N_2 \rightarrow O(^3P) + N_2 \quad (6)$$

system A,

$$I_2 + Br_2 \leftrightarrow 2IBr \quad (7)$$

$$O(^3P) + IBr \rightarrow IO + Br \quad (8a)$$

$$\rightarrow BrO + I \quad (8b)$$

$$O(^3P) + Br_2 \rightarrow BrO + Br \quad (9)$$

system B,

$$O(^3P) + IBr \rightarrow IO + Br \quad (8a)$$

$$\rightarrow BrO + I \quad (8b)$$

system C,

$$O(^3P) + CF_3I \rightarrow IO + CF_3 \quad (10)$$

$$O(^3P) + Br_2 \rightarrow BrO + Br \quad (9)$$

In system A, equilibrium between I_2, Br_2, and IBr was achieved prior to photolysis. Prior to equilibration, Br_2 concentrations were approximately 30-fold in excess over I_2, thus following equilibration $[I_2]$ was low and reaction 11 made a negligible contribution to the generation of IO:

$$O(^3P) + I_2 \rightarrow IO + I \quad (11)$$

In system B, I_2 and Br_2 were present in equilibrium with IBr, thus reactions reactions 9 and 11 also occurred; however, the relative concentrations of I_2, Br_2, and IBr were such that reaction 8 dominated IO and BrO production.

N_2O (Distillers MG, 99%), N_2 (Distillers MG, 99.996%), and O_2 (Distillers MG, 99.996%) were used as supplied. I_2 (Breckland Scientific, resublimed) and IBr (Lancaster, 98%) were entrained in a flow of N_2 passed through bulbs containing halogen flakes interspersed with glass wool. Br_2 was entrained in a flow of nitrogen passed through a bromine bubbler, which was held in an ice bath to ensure a known and convenient vapor pressure. CF_3I (Fluorochem, 99%) was taken directly from a pressure cylinder. Concentrations of precursor species entering the reaction cell are given in Table 2. In all cases, precursor concentrations were such that O atoms reacted rapidly and exclusively with halogen species. Concentrations of N_2 and CF_3I were calculated from their known flow rates, and those of I_2, Br_2, and IBr from flow rates and the appropriate vapor pressures. For system A, at typical I_2 and Br_2 concentrations prior to mixing of 3×10^{14} and 1×10^{16} molecules cm^{-3}, respectively, I_2 was calculated to be overwhelmingly (98.9%) converted to IBr, using the equilibrium constant for reaction 7 of 20.19 at 298 K,[29] if iodine and bromine had equilibrated. Evidence that equilibrium between I_2 and Br_2 was attained was provided by tests in which the contact time for I_2 and Br_2 was reduced to approximately 30% of that used in the subsequent kinetic experiments, and the concentration of Br_2 was reduced by a factor of 15. Under these conditions, the presence of bromine reduced the I_2 concentration by 85%, indicating that under the normal experimental conditions, equilibrium between I_2, Br_2, and IBr was effectively complete.

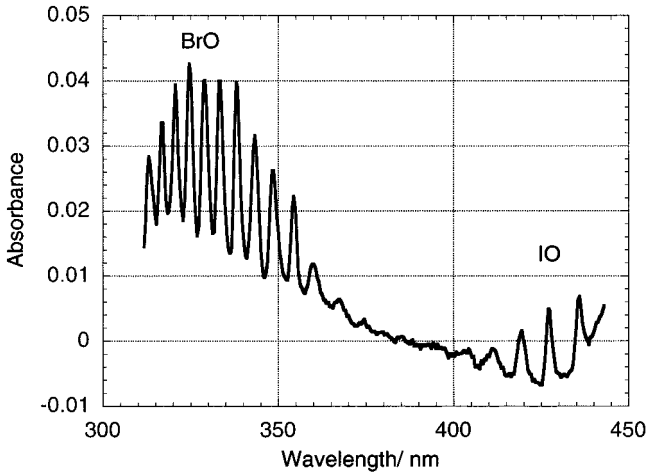

Figure 1. Post-photolysis absorption spectrum recorded using system C (Br_2/CF_3I). The spectrum is a postrelative (I_t) to prephotolysis (I_o) spectrum, showing changes in absorption bought about by the photolysis flash and subsequent chemistry. Thus, the negative baseline above 380 nm arises from the consumption of Br_2 in the postphotolysis reactions.

The use of different precursor mixtures facilitated the investigation of different aspects of the IO + BrO reaction system: System A was used to investigate the kinetics of the IO + BrO reaction, system B was used to constrain the branching ratio for the O + IBr reaction, and system C was used to investigate the products of reaction 1, and to test qualitative understanding of the secondary chemistry occurring. System A was used for kinetic measurements as the I_2 and Br_2 concentrations could be independently adjusted to attain the initial [IO]:[BrO] ratio which maximized the sensitivity of the IO and BrO decay traces to the IO + BrO reaction rate coefficient; such control was not possible with system B. System C was not used for kinetic experiments as the presence of CF_3 and CF_3I, the reactions of which with IO and BrO are not well characterized, could introduce errors arising from secondary chemical interactions.

Radical Monitoring. IO and BrO radicals were monitored via their characteristic structured UV−vis absorption spectra arising from the characteristic $A^2\Pi \leftarrow X^2\Pi$ vibronic transition. Spectrograph settings (150 g/mm grating and 50 μm entrance slit width) corresponded to coverage of the wavelength range 315−445 nm at a resolution (fwhm) of 1.65 nm, and permitted simultaneous detection of IO and BrO. A typical postphotolysis absorption spectrum, recorded using the CF_3I/Br_2 system C, is shown in Figure 1.

Concentrations of IO and BrO radicals were determined by fitting reference cross sections over the wavelength ranges 400−445 and 315−360 nm, respectively, using the technique of differential spectroscopy. The magnitude of the vibronic features manifest in the absorption spectra of species such as halogen monoxide radicals is dependent upon the instrumental resolution used, and the cross sections used to quantify such species must therefore be recorded at the appropriate resolution, or smoothed from higher resolution measurements. Reference IO cross sections were recorded at 1.65 nm fwhm resolution, following

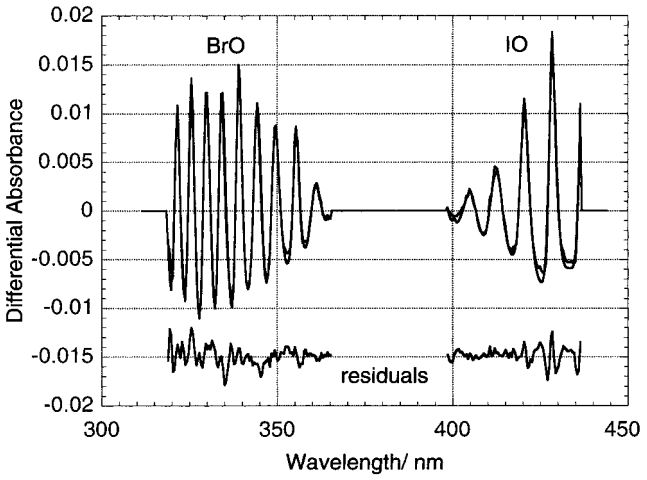

Figure 2. Differential fit of BrO and IO reference cross sections to a post-photolysis absorption spectrum, with residuals (offset). Fits independently quantify [IO] and [BrO] at each time point

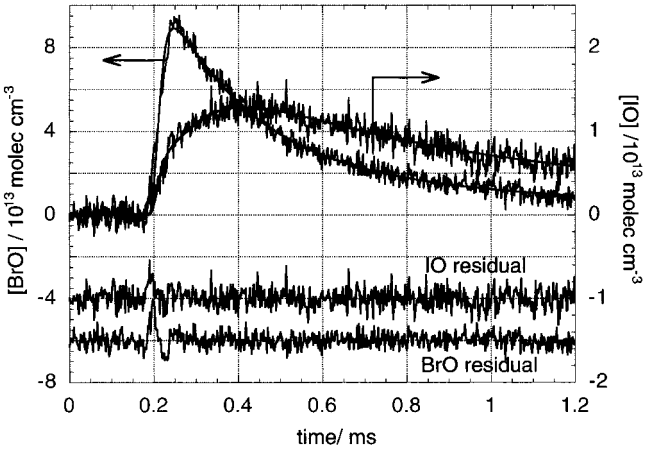

Figure 3. IO and BrO concentration−time profiles (decay traces), optimized fits and residuals (offset), obtained using system A ($I_2/Br_2/N_2O/N_2$).

photolysis of $CF_3I/N_2O/N_2$ mixtures. These cross sections were calibrated by carrying out parallel experiments performed at higher (1.13 nm fwhm) resolution, using the IO cross sections reported at this resolution in the accompanying paper.[1] Wavelength-dependent BrO cross sections have been measured by Wahner et al.[30] Gilles et al.[20] have recently remeasured the differential BrO cross section around 338 nm, and found it to be approximately 9% larger than that reported by Wahner et al. Gilles et al. noted that making a corresponding correction to rate coefficients for the BrO self-reaction measured via UV-absorption detection of BrO using the cross sections of Wahner et al. brought such results into agreement with those performed using other techniques. The BrO cross sections used in this work were those measured by Wahner et al., increased in magnitude by 9% in line with the findings of Gilles et al., and smoothed to the resolution used in this study. A typical differential fit to the IO and BrO absorption features in a postphotolysis absorption spectrum is shown in Figure 2.

The CCD was operated at a charge-transfer rate of 5×10^5 Hz, corresponding to recording an absorption spectrum of the reaction mixture every 2 μs, for a period of 1 ms following photolysis. Fitting of IO and BrO cross sections to successive absorption spectra determined IO and BrO decay traces such as those shown in Figure 3, obtained using system A.

3. Results

Products of the O + IBr Reaction. The branching ratio θ for IO production in reaction 8, is defined by $\theta = k_{8a}/(k_{8a} + k_{8b})$ and was measured using system B, $N_2O/IBr/N_2$. Peak IO and BrO concentrations observed immediately after photolysis were found to be in the ratio 83%:17%, or 4.75:1. These values do not allow direct calculation of the branching ratio for reaction 8, however, as IO and BrO are also formed from the reaction of O atoms with I_2 and Br_2, respectively, which were present in equilibrium with IBr. While the I_2, Br_2, and IBr concentrations present in the reaction cell could be calculated, the rate coefficient for the O + IBr reaction is not known. Thus, the flux of O atoms reacting with IBr could not be ascertained, precluding determination of the branching ratio for reaction 8 other than in terms of k_8.

In system B, in which I_2 and Br_2 are present in equal concentrations in equilibrium with IBr, the observed initial ratio of [IO]:[BrO], R, relates θ and k_8 as shown in eq ii, where K_8 is the equilibrium constant for reaction 8:

$$R = \frac{(k_{11} + k_8\theta\sqrt{K_8})}{(k_9 + k_8(1-\theta)\sqrt{K_8})} \qquad \text{(ii)}$$

Using the observed value of 4.75 for R, eq ii indicated that the value of θ is relatively insensitive to the value of k_8, varying between 0.6 and 0.8 for $k_8 = 2 \times 10^{-11}$ to 1.4×10^{-10} molecules^{-1} cm^3 s^{-1} (the range encompassed by the O + Br_2 and O + I_2 reaction rate coefficients, respectively.[31]) The O + IBr reaction rate coefficient is expected to lie between the O + I_2 and O + Br_2 reaction rate coefficients (as has been observed for O + BrCl and O + ICl, by (e.g.) Lowenstein et al.[32]), indicating a value of ca. 5×10^{-11} molecules^{-1} cm^3 s^{-1} for k_8, corresponding to a value of 0.7 for θ. This value was used in the reaction system model used to determine the kinetics of the IO + BrO reaction. The dependence of the results obtained upon the value assumed for θ is discussed below.

Kinetics of the IO + BrO Reaction. IO and BrO decay traces recorded using system A, $I_2/Br_2/N_2O/N_2$, were analyzed to determine kinetic data using a model of the reaction system constructed in FACSIMILE.[33] The model incorporated simulations of photolysis, flowout, the temporal distortion imparted to decay traces by CCD oversampling and the chemical reaction scheme given in Table 3. Within the model, the initial O atom concentration, $[O(^1D)]_{t=0}$, and the values of k_1 (IO + BrO), k_{12} (I + BrO), and k_8 (O + IBr) were optimized by minimizing the sum of squares of residuals between observed and calculated IO and BrO decay traces. The sensitivity of the kinetic results so obtained to the secondary chemical reactions incorporated in the model, and the choice of kinetic parameters optimized, is discussed in the following section.

Reaction System Model: Sensitivity Tests. Sensitivity tests were performed using the reaction model in order to determine which of the reactions occurring had a significant impact upon the form of the IO and BrO decay traces (i.e., which reaction rate coefficients could be determined from IO and BrO concentration−time data). Sensitivity tests were then used to establish the dependence of the values of rate coefficients determined upon the correct implementation of the secondary chemical reactions (i.e., the sensitivity of the optimized rate coefficients to other reactions in the model.)

The first test was performed by measuring the deviation between simulated decay traces generated using the reaction scheme for system A implemented as shown in Table 3 (control

TABLE 3: Secondary Chemical Reaction Scheme, and Appropriate Rate Coefficients (for 295 K/760 Torr), Employed in the Reaction System Model

reaction	reaction no.	295 K rate coeff[a]/ cm^3 molecule^{-1} s^{-1}	ref
$O(^1D) + N_2 \rightarrow O(^3P) + N_2$	6	2.61×10^{-11}	42
$O(^3P) + IBr \rightarrow IO + Br$	8a	3.5×10^{-11}	
$O(^3P) + IBr \rightarrow BrO + I$	8b	1.5×10^{-11}	
$O(^3P) + Br_2 \rightarrow BrO + Br$	9	1.4×10^{-11}	31
$O(^3P) + IO \rightarrow I + O_2$		1.4×10^{-10}	42
$O(^3P) + BrO \rightarrow Br + O_2$		4.1×10^{-11}	42
$IO + BrO \rightarrow$ products	1	6.9×10^{-11}	
$I + BrO \rightarrow IO + Br$	12	1.9×10^{-11}	39
$Br + IO \rightarrow BrO + I$	13	5×10^{-11}	39
$IO + IO \rightarrow$ products	14	8.18×10^{-11}	1
$BrO + BrO \rightarrow$ products		2.98×10^{-12}	28
$I + Br_2 \rightarrow IBr + Br$	15	3.4×10^{-13}	44
$Br + I_2 \rightarrow IBr + I$	16	1.38×10^{-14}	38
$Br + IBr \rightarrow Br_2 + I$	17	4.6×10^{-11}	45
$I + IO \rightarrow I_2O$		1.7×10^{-10}	1
$I + I_2O \rightarrow I_2 + IO$		2.1×10^{-10}	1
$Br + BrO + M \rightarrow Br_2O + M$		3×10^{-12}	13
$Br + Br_2O \rightarrow Br_2 + BrO$		2×10^{-10}	46
$I + I \rightarrow I_2$		2.47×10^{-13}	47
$Br + Br \rightarrow Br_2$		7.6×10^{-14}	48

[a] Rate coefficients for reactions 1, 8, and 12 were optimized when fitting to experimental IO and BrO concentration profiles; the values for k_1, k_8, and k_{12} listed above are those used for sensitivity tests. I and Br atom recombination rate coefficients are reported at 760 Torr of N_2.

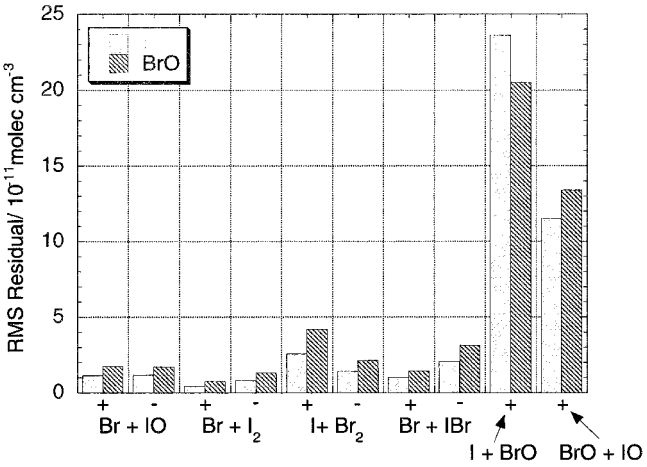

Figure 4. Sensitivity test 1. The sensitivity of the form of the IO and BrO decay traces to perturbations of the rate coefficient of each reaction occurring.

decay traces), and those generated when the rate coefficient for each reaction was perturbed, in turn, by an arbitrary factor of ± 50%. The deviation between perturbed and control decay traces was evaluated as the RMS residual for each species, IO and BrO, calculated over the 1 ms postphotolysis time period corresponding to our experimental conditions. The results of this test (plotted in Figure 4) show clearly that the IO and BrO decay traces exhibit similar patterns of sensitivity, displaying the greatest dependence upon the rate coefficient for the I + BrO reaction 12 followed by the IO + BrO reaction 1. Sensitivity to the other reactions taking place was considerably lower: In particular, the traces displayed very little sensitivity to the rate coefficient for reaction 13, Br + IO, due to the conversion of Br atoms to I atoms, predominantly through the halogen/interhalogen atom−molecule reactions.

$$I + BrO \rightarrow IO + Br \quad (12)$$

$$Br + IO \rightarrow BrO + I \quad (13)$$

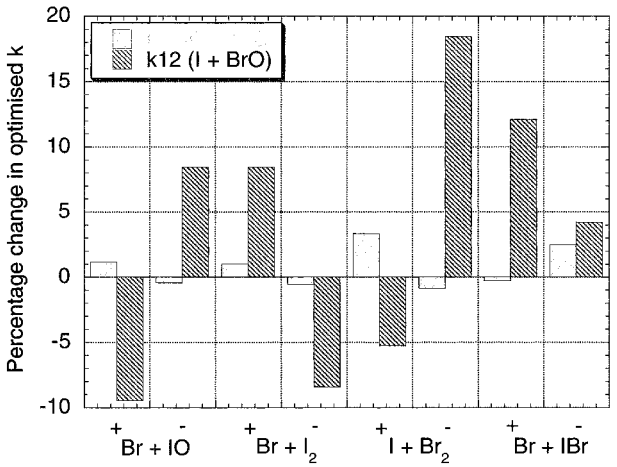

Figure 5. Sensitivity test 2. The sensitivity of the optimized values of k_1 and k_{12} to the rate coefficient of selected secondary reactions included in the reaction model.

Similar tests indicated that the decay traces were relatively insensitive to the branching ratios for the IO + IO and IO + BrO reactions. Decay trace sensitivity to k_1 (the IO + BrO reaction) was found to maximize when the initial BrO concentration was approximately three times that of IO.

The second test determined the dependence of the optimized rate coefficients upon the secondary chemical reactions. The rate coefficient for each secondary reaction, in turn, was perturbed by ± 50%, and this perturbed reaction model used to generate IO and BrO decay traces. The original model (as given in Table 3) was then used to re-analyze these traces, determining an optimized value for k_1 only. The difference between this optimized value of k_1 and the value used in the perturbed model (6.9×10^{-11} molecules^{-1} cm^3 s^{-1}, as measured by Laszlo et al.[19]) gave an indication of the sensitivity of the optimization of k_1 to each secondary reaction in the model.

The returned value of k_1 was found to exhibit moderate sensitivity to many of the secondary chemical reactions incorporated in the model, typically varying by 20% for each 50% perturbation of a secondary reaction rate coefficient. Noting that the IO and BrO decay traces exhibited strong dependence upon both k_1 and k_{12}, the second sensitivity test was repeated optimizing both k_1 and k_{12} to fit the artificial IO and BrO decay traces. In this case, the sensitivity of k_1 to the secondary reactions was much reduced; typically, k_1 varied by less than 5% for each 50% perturbation of a secondary reaction rate coefficient. The sensitivity of k_{12} was somewhat greater, varying by up to 20% for the same degree of perturbation. The results from these dual-optimization tests are plotted in Figure 5, which shows the percentage change in the reoptimized k_1 and k_{12} for the 50% perturbation of each secondary reaction rate coefficient.

The insensitivity of the returned values of k_1 and k_{12} to secondary chemistry, as determined by the dual-optimization analysis, was verified by investigating the nature of the error surface defined by the fits to the IO and BrO decay traces. Control IO and BrO decay traces were generated using the nominal values for these rate coefficients, and compared with those obtained when the values of k_1 and k_{12} were altered by some factor. The deviation between traces was defined as the sum of the RMS residuals for each species (IO and BrO) over the 1 ms post-photolysis time-period. This quantity was expressed as a function of k_1 and k_{12}, varying both rate coefficients by a factor of 3, and generating a "goodness of fit" error matrix. This is shown in Table 4, and the presence of a single minimum value for the residual indicates that a unique

TABLE 4: Sensitivity Test for k_1 and k_{12}[a]

	factor Change in k_1				
factor change in k_{12}	0.333	0.5	1	2	3
3	11.4	11.4	12.2	14.6	16.9
2	7.0	4.8	5.6	8.5	11.2
1	4.0	1.4	0	1.7	6.0
0.5	22.2	16.4	8.1	4.3	8
0.3333	17.0	16.0	15.0	13.1	10.7

[a] Change in the RMS residual on decay traces resulting from deviations in k_1 and k_{12} values from optimized values.

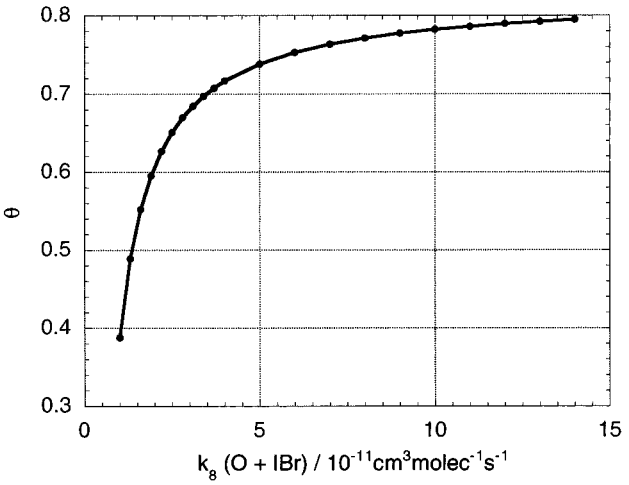

Figure 6. Relationship between value of k_8 obtained by optimization and value of the branching ratio for reaction 8, θ, used in the optimization model.

pair of values for k_1 and k_{12} best described the IO and BrO decay traces. Hence k_1 and k_{12} were both independently determinable from the IO and BrO decay traces.

In addition to k_1 and k_{12}, the value of k_8 (O + IBr) was optimized in the reaction model. The value obtained for k_8 was determined by the initial [IO]:[BrO] ratio, as all O atoms were consumed rapidly (with a total pseudo-first-order half-life ranging from 3 to 25 μs dependent upon conditions), and thus did not impact upon the subsequent form of the IO and BrO decay traces, which determined the values of k_1 and k_{12}.

Kinetic Results Ambient Conditions. Figure 3 shows IO and BrO decay traces, optimized fits and residuals (offset) typical of those used to determine the values of k_1, k_{12}, and k_8. At ambient temperature (295 ± 3 K) and at 760 Torr total pressure, these rate coefficients were found to be

$$k_1\,(\mathrm{IO} + \mathrm{BrO}) = (8.5 \pm 1.4) \times 10^{-11}\ \mathrm{molecules}^{-1}\,\mathrm{cm}^3\,\mathrm{s}^{-1}$$

$$k_{12}\,(\mathrm{I} + \mathrm{BrO}) = (1.3 \pm 1.2) \times 10^{-11}\ \mathrm{molecules}^{-1}\,\mathrm{cm}^3\,\mathrm{s}^{-1}$$

$$k_8\,(\mathrm{O} + \mathrm{IBr}) = (3.6 \pm 2.4) \times 10^{-11}\ \mathrm{molecules}^{-1}\,\mathrm{cm}^3\,\mathrm{s}^{-1}$$

Errors are 2σ and represent precision only: Values were obtained from the analysis of 33 experiments conducted over the precursor concentration ranges indicated in Table 2, each the coaddition of 50 or 100 laser shots.

The value obtained for k_8 was entirely dependent upon the branching ratio θ ($= k_{8a}/k_8$) employed in the reaction system model (the value of 0.7 was used for θ to obtain the above value for k_8). These experiments were thus limited to establishing that k_8 and θ are related as shown in Figure 6; independent determination of either k_8 or θ was not possible from our data.

TABLE 5: Pressure Dependence of k_1[a]

pressure/Torr	$k_1/10^{-11}$ molecules^{-1}cm^3 s^{-1}
100	8.30 ± 0.98
220	7.54 ± 1.48
360	8.14 ± 0.25
480	8.24 ± 1.30
600	8.82 ± 0.65
760	8.50 ± 1.40

[a] Uncertainties are 2σ.

TABLE 6: Values of k_1, k_{12}, and k_8 Obtained as a Function of Temperature[a]

	IO + BrO		I + BrO		O + IBr	
temperature/K	k_1	$\pm 2\sigma$	k_{12}	$\pm 2\sigma$	k_8	$\pm 2\sigma$
333	6.81	0.39	1.59	0.06	4.62	1.08
296	8.49	1.40	1.30	1.27	3.57	2.48
283	11.03	0.23	1.06	0.01	5.38	0.57
273	10.08	0.73	1.48	0.04	7.91	0.67
260	13.70	0.49	1.00	0.05	7.48	1.12
250	16.82	2.92	1.38	0.16	7.54	5.04
235	19.44	4.75	1.17	0.20	14.98[b]	2.98
222	18.67	1.27	0.63	1.27	6.52	1.62
210	21.17	2.91	0.30	0.02	4.00	0.76

[a] Units: molecules^{-1} cm^3 s^{-1} × 10^{-11}. [b] Excluded from subsequent analysis.

Kinetic Results Pressure and Temperature Dependence. Experiments were conducted over a range of pressures, between 100 and 760 Torr. At ambient temperature, k_1, k_{12}, and k_8 were found to be pressure-independent over this range. The invariance of k_1 with pressure is shown in Table 5.

Experiments were conducted as a function of temperature, between 210 and 333 K. The rate coefficients of the secondary reactions included in the optimization model were adjusted to their appropriate temperature-dependent values as given in the references indicated in Table 3. Exceptions to this were the branching ratios for the IO + IO and IO + BrO reactions, and the rate coefficients for reactions 13 and 15−17. These parameters, the temperature dependencies of which are not known, were fixed at their 295 K values. The insensitivity of the value obtained for k_1 upon these parameters (Figure 5) indicated that the use of the model to determine the value of k_1 at temperatures other than ambient was valid; however, the optimized value of k_{12} was approximately 4-fold more sensitive to the secondary chemical scheme than k_1, implying somewhat reduced confidence in the temperature-dependent values of this rate coefficient. The value determined for k_9 was solely dependent upon the initial IO and BrO concentrations, and thus was not susceptible to incomplete implementation of the temperature dependence of the secondary chemistry. However, the analysis did not take account of possible variation in the branching ratio θ of reaction 8 with temperature.

The values obtained for k_1, k_{12}, and k_8 as a function of temperature are given in Table 6. The value of k_1 (IO + BrO) was found to increase with decreasing temperature, in a manner which could be described by an Arrhenius expression:

$$k_1 = (6.7 \pm 0.8) \times 10^{-12} \exp((760 \pm 30)/T)\ \mathrm{molecules}^{-1}\,\mathrm{cm}^3\,\mathrm{s}^{-1} \quad \text{(iii)}$$

Error limits correspond to $\pm 2\sigma$ and represent precision only. The values of k_1 are plotted as a function of temperature in Figure 7, together with the temperature-dependent results obtained by Gilles et al.[20] and the 298 K results of Bedjanian et al.[21] and Laszlo et al.[19]

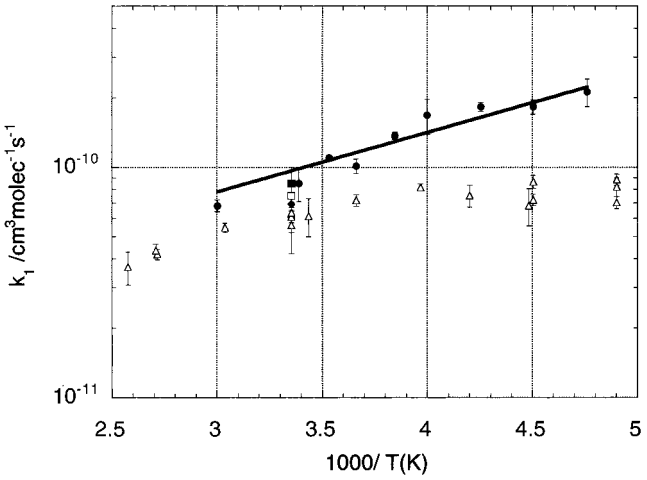

Figure 7. Temperature-dependent values for k_1 obtained in this work (filled circles) compared with the results of Gilles et al.[20] (open triangles), Laszlo et al.[19] (open squares), and Bedjanian et al.[21] (filled squares). The line is an Arrhenius fit to k_1 (this work).

The value of k_8 (O + IBr) displayed no significant variation with temperature (within the precision of the measurements) over the range studied, leading to an unweighted mean value of $(4.6 \pm 1.8) \times 10^{-11}$ molecules^{-1} cm^3 s^{-1} (210−333 K; $\pm 2\sigma$). k_{12} was also found to be temperature independent at 235 K and above; over this range, the unweighted mean value obtained was $(1.3 \pm 0.4) \times 10^{-11}$ molecules^{-1} cm^3 s^{-1} ($\pm 2\sigma$). At lower temperatures (210 and 222 K), the value of k_{12} obtained was significantly smaller. The temperature-dependent values of k_8 and k_{12} are given in Table 6.

Products of the IO + BrO Reaction. Each of the five potential product channels of the IO + BrO reaction is considered in turn.

(a) I + Br + O_2. It was not possible to detect I or Br atoms directly using our experimental system. The addition of ozone to the reaction system, leading to the reconversion of the X (X = Br, I) atoms to XO radicals, and hence to a reduction in the observed rate coefficient for the IO + BrO reaction, would have allowed quantification of halogen atom production. However, when preliminary experiments were conducted in which O_3 was added to the precursor gas mixture, powdery yellow-white deposits formed upon the surfaces of the gas manifold and reaction cell. These deposits were similar in appearance to those formed when O_3 and molecular iodine were brought into contact,[1] and are likely to have been the same higher oxides of iodine, I_2O_4, I_2O_5, and/or I_4O_9, formed in this case following reaction between O_3 and IBr. The formation of these deposits on the optical surfaces of the system precluded the conduct of useful experiments in the presence of ozone; it was not therefore possible to quantify channel 1a directly.

(b) IBr + O_2. Investigation of the production of IBr from the IO + BrO reaction was complicated by the presence of this species at significant levels in the precursor gas mixtures employed. Experiments were conducted using system C, Br_2/CF_3I, in which the production of IBr, monitored spectroscopically, was compared with the modeled flux through the IO + BrO reaction. The IBr concentrations observed indicated a branching ratio for this channel of the order of 0.2 (i.e., $k_{1b}/k_1 \approx 0.2$); however, several other potential sources of IBr existed, notably the I + Br_2 and possibly the Br + CF_3I[34] reactions. The magnitude of the contributions of these reactions to the observed IBr could not be calculated with certainty, thus the value obtained determines an upper limit for production of IBr from the IO + BrO reaction, $k_{1b}/k_1 \leq 0.2$.

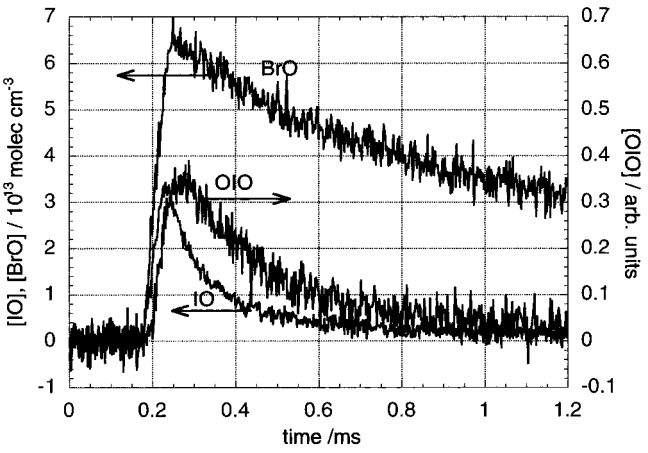

Figure 8. IO, BrO, and OIO decay traces, recorded using system C ($CF_3I/Br_2/N_2O/N_2$). The OIO trace was obtained by differential fitting to an uncalibrated OIO absorption spectrum.

(c) OIO + Br. Growth and decay of the distinctive absorption bands of OIO between 500 and 600 nm were observed in the post-photolysis spectra of the IO + BrO reaction system. Differential spectral fitting to an arbitrary OIO absorption spectrum was used to obtain absorption−time profiles for OIO, revealing behavior qualitatively similar to that observed in the IO self-reaction:[1] OIO was a transient species, forming and decaying on a time scale similar to that of the IO radical. IO and BrO concentration profiles, and an OIO absorption profile, are shown in Figure 8, recorded using the CF_3I/Br_2 system C. OIO is known to be a product of the IO self-reaction,[1] which also occurred in the IO + BrO reaction system. Moreover the ratio of OIO:IO was similar to that observed in our studies of the IO self-reaction. However, in the IO + BrO system, the fraction of IO radicals reacting with BrO was much greater (3−4 times) than that undergoing self-reaction; therefore, the observation of similar OIO:IO ratios indicates that OIO is also a product of the IO + BrO reaction. Further analysis which constrains the branching ratio for OIO production from the IO + BrO and IO + IO reactions and hence its absorption cross section is described below.

(d) OBrO + I. No evidence for the formation of OBrO was observed in the course of this work. On the basis of the estimated cross section for OBrO of 1.5×10^{-17} molecules^{-1} cm^2 at 505.7 nm,[35] we determine an upper limit for channel 1d of $k_{1d}/k_1 \leq 0.15$.

(e) $IBrO_2$. No spectroscopic evidence was observed for the presence of any absorbing species other than the XO radicals, the products of the IO self-reaction, OIO from IO + BrO and the halogen and interhalogen molecules, at any of the temperatures investigated in the course of this work (210−333 K). No evidence for the formation of an $IBrO_2$ species was observed. The pressure independence of the IO + BrO reaction rate coefficient between 760 Torr (this work) and 1 Torr[21] indicates that termolecular $IBrO_2$ formation does not occur. Similarly, no evidence for $IBrO_2$ formation has been observed in previous studies of the IO + BrO reaction.[19,20]

Yield of OIO from IO + BrO and IO + IO. The branching ratio for production of OIO from reaction 1 was constrained by considering the results obtained in this work in conjunction with those reported elsewhere. Bedjanian et al.[21] have determined the branching ratio for the production of OIO from the IO + BrO reaction to be equal to or in excess of 0.65; i.e. $0.65 \leq k_{1c}/k_1 \leq 1$. Bedjanian et al. also placed upper limits for the formation of I + Br + O_2, IBr + O_2 and OBrO + I of $k_{1a}/k_1 \leq 0.5$, $k_{1b}/k_1 \leq 0.05$ and $k_{1d}/k_1 \leq 0.2$, respectively. Gilles et al.[20]

measured the rate coefficient for the non I atom producing channels of reaction 1, i.e., $k_{obs} = k_{1b} + k_{1c}$, assuming $k_{1e} = 0$. Comparison of the value obtained by Gilles et al. at 298 K, $k_{obs} = (6.05 \pm 0.57) \times 10^{-11}$ molecules^{-1} cm^3 s^{-1}, with the value of k_1 obtained in this work, $(8.5 \pm 1.4) \times 10^{-11}$ molecules^{-1} cm^3 s^{-1}, indicates that channels 1b and 1c, IBr + O_2 and OIO + Br, account for 55 to 93% of the IO + BrO reaction, i.e., $0.55 \leq (k_{1b} + k_{1c})/k_1 \leq 0.93$, where the range corresponds to the 2σ uncertainty level in the kinetic results. The range common to this analysis and the results of Bedjanian et al. thus determines $0.65 \leq k_{1c}/k_1 \leq 0.93$.

The branching ratio for OIO production from the IO + BrO reaction was used to quantify the production of OIO from the IO self-reaction, and so to determine the absolute absorption cross sections of OIO. The branching ratio for the production of OIO from the IO self-reaction and the IO + BrO reaction, denoted α and β respectively, are defined by

$$\mathrm{IO} + \mathrm{IO} \rightarrow \mathrm{OIO} + \mathrm{I} \quad (14a)$$

$$\rightarrow \text{other products} \quad (14b)$$

$$\alpha = k_{14a}/k_{14} \quad \text{(iv)}$$

$$\beta = k_{1c}/k_1 \quad \text{(v)}$$

The concentration of reactant molecules (IO and BrO) is known in both the IO self-reaction and IO + BrO reaction systems. Because the IO + IO and IO + BrO overall rate coefficients are also known, the flux through each of these reactions can be evaluated, and the production rate of OIO calculated in terms of α and β in each system:

$$\text{OIO production rate } P_{OIO} = \alpha k_{14}[\mathrm{IO}]^2 (\mathrm{IO} + \mathrm{IO} \text{ system}) \quad \text{(vi)}$$

$$\text{OIO production rate } P_{OIO} = \alpha k_{14}[\mathrm{IO}]^2 + \beta k_1[\mathrm{IO}][\mathrm{BrO}](\mathrm{IO} + \mathrm{BrO} \text{ system}) \quad \text{(vii)}$$

The total concentration of OIO formed at any point following photolysis, neglecting OIO loss processes, is then given by the integral of P_{OIO} with respect to time. Two equations were therefore derived, one from each system, relating the calculated OIO production to the observed OIO absorption A in terms of the OIO cross section σ_{OIO}:

$$A_a/(\sigma_{OIO}\,\mathrm{L}) = \int \alpha k_{14}[\mathrm{IO}]_a^2 \quad \text{(viii)}$$

$$A_b/(\sigma_{OIO}L) = \int \{\alpha k_{14}[\mathrm{IO}]_b^2 + \beta k_1[\mathrm{IO}]_b[\mathrm{BrO}]_b\} \quad \text{(ix)}$$

where the subscripts a and b refer to measurements made in the IO + IO and IO + BrO reaction systems respectively, and L is the absorption path length. Equations viii and ix were thus solved to determine α and σ_{OIO} in terms of β, which is known to lie in the range $0.65 \leq \beta \leq 0.93$. This analysis neglects the chemical reactions responsible for the rapid removal of OIO observed in both reaction systems, and thus was only applied at very short times following photolysis, when IO and BrO concentrations maximize and the OIO concentration is dominated by production. The values of α derived by this method are plotted, as a function of the value of β used and of time following photolysis, in Figure 9. The values of α at very short times are obscured by noise in the retrieval of the (initially low) IO and BrO concentrations, then settle as the IO + IO and IO + BrO reaction rates maximize, before increasing as the loss processes of OIO become of increasing importance relative to production. The increase in α beyond 0.07 s reflects the greater loss processes for OIO present in the more chemically diverse IO + BrO reaction system. In practice the time period when both the IO + IO and IO + BrO reaction rates were within 10% of their maximum values was used to determine α and hence σ_{OIO}; this time period is indicated in Figure 9. The range of values determined for α and σ_{OIO} are

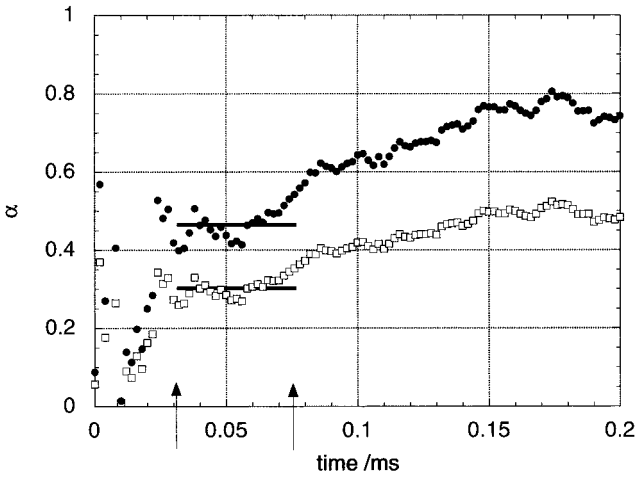

Figure 9. Values of α (branching ratio for production of OIO from IO + IO) as a function of time after photolysis, calculated for β (branching ratio for production of OIO from IO + BrO) = 0.65 (open squares) and 0.93 (filled circles).

TABLE 7: Comparison of Literature Values for k_1 with the Results of This Work

authors	date	k_1 (298 K) × 10^{11}, molecules^{-1}cm^3 s^{-1}	technique[b]
Laszlo et al.[19]	1997	6.9 ± 2.7	LFP/UVA
Gilles et al.[20]	1997	6.05 ± 0.57[a]	DF/LFP/UVA/LIF
Bedjanian et al.[21]	1998	8.5 ± 1.5	DF/MS
this work	1999	8.49 ± 1.40	LFP/UVA

[a] Measured only the non-I atom producing channels of reaction 1. [b] LFP = laser flash photolysis, UVA = UV absorption spectroscopy, DF = discharge flow, LIF = laser-induced fluorescence, MS = mass spectrometry.

$$0.30 \pm 0.05 \leq \alpha \leq 0.46 \pm 0.08$$

and $1.29 \pm 0.22 \geq \sigma_{OIO} \times 10^{17} \geq 0.87 \pm 0.15$ cm^2 molecules^{-1}

where the range corresponds to $0.65 \leq \beta \leq 0.93$, and the errors quoted correspond to 2σ limits in the determinations. σ_{OIO} was evaluated at 549 nm and the peak of the (5,1,0) band[36] at 1.13 nm fwhm resolution. OIO production thus accounts for 30−46% of the IO self-reaction, in addition to being the major product of the IO + BrO reaction. The products of the IO self-reaction are considered in detail in the accompanying paper[1] in light of this result.

4. Discussion

There have been three recent studies of the IO + BrO reaction reported in the literature, the results from which are summarized in Table 7. The rate coefficient obtained for the overall IO + BrO reaction in this work is in excellent agreement with the value reported by Bedjanian et al.[21] The overall rate coefficient is also within the range obtained by Gilles et al.,[20] who obtained a value of 6.05×10^{-11} molecules^{-1} cm^3 s^{-1} for $(k_{1b} + k_{1c})$ at 298 K, and determined that the I atom production was ≤35%,

indicating an upper limit for k_1 at 298 K of 1.0×10^{-10} molecules^{-1} cm^3 s^{-1}. The rate coefficient obtained in this work is slightly higher than the value of $(6.9 \pm 2.7) \times 10^{-11}$ molecules^{-1} cm^3 s^{-1} obtained by Laszlo et al.[19] using a similar experimental system; this discrepancy is partially due to the BrO cross sections used: Laszlo et al. employed the BrO cross sections measured by Wahner et al.,[30] but without the increased magnitude recently recommended by Gilles et al.[20] Making this adjustment to the value of k_1 reported by Laszlo et al. would increase the value by approximately 10%, bringing the two studies into better agreement.

The results reported in this paper were obtained using the BrO cross sections of Wahner et al.,[30] increased in magnitude by 9% in line with the findings of Gilles et al.,[20] to analyze spectroscopic data and determine [BrO]. After our analysis, Wilmouth et al.[37] have published further measurements of the BrO absorption spectrum, including a comprehensive review of the BrO absorption cross sections. They report a mean differential BrO cross section, obtained from a comparison of literature results normalized for resolution, which is approximately 13% smaller than that used in this work. Adoption of such a σ(BrO) would reduce our measured k_1, by somewhat less than 10%, as the XO kinetics in our system are complex. Such a change would also increase the deduced OIO yield from both the IO + BrO and IO + IO reactions. Wilmouth et al. determined an uncertainty of 11% in the literature differential BrO cross sections, independent of temperature. The IO cross sections used in this work have an uncertainty of 9%.[1] We therefore estimate that the component of the systematic uncertainty in our kinetic measurements which arises from the cross sections used is approximately 15%, considering the dependence of the value obtained for k_1 upon absolute concentrations of both species.

The measurement of $k_{1b} + k_{1c}$ performed by Gilles et al.[20] together with the measurement of k_1 reported in this work determine a value for the branching ratio for channels 1b and 1c of the IO + BrO reaction, $\{k_{1b} + k_{1c}\}/k_1$, which is in very good agreement with the range determined by Bedjanian et al.[21] at 298 K. Taken together, these values lead to a range of 0.65−0.93 for k_{1c}/k_1. Bedjanian et al. also obtained upper limits for channels 1a, 1b, and 1d, of which the latter has been further reduced to 0.15 in this work. No evidence for channel 1e has been observed. The results of all recent studies constrain the branching ratios for the IO + BrO reaction at 298 K to

$$\mathrm{IO + BrO} \rightarrow \mathrm{I + Br + O_2} \leq 0.3 \quad (1a)$$

$$\rightarrow \mathrm{IBr + O_2} \leq 0.05 \quad (1b)$$

$$\rightarrow \mathrm{OIO + Br} \quad 0.65-0.93 \quad (1c)$$

$$\rightarrow \mathrm{OBrO + I} \leq 0.15 \quad (1d)$$

$$\rightarrow \mathrm{IBrO_2} \quad (1e)$$

Comparison of the temperature-dependent results of this work with those of Gilles et al.[20] (Figure 7) indicates that the branching ratio for the non-I atom producing channels of reaction 1, 1b, and 1c decreases with decreasing temperature, from 71% at 295−298K to 36% at 210 K. The branching ratio of channels 1a and/or 1d therefore increases with decreasing temperature. Because no evidence for OBrO formation has been observed, and this channel is calculated to be considerably endothermic at 298 K, it is possible that channel 1a, I + Br + O_2, dominates the IO + BrO reaction at low temperatures: If indeed channel 1d does not occur, $k_{1a} = 1.6 \times 10^{-10}$ molecules^{-1} cm^3 s^{-1} at 210 K. This analysis assumes that the branching ratio of the IO + BrO reaction is invariant over the pressure range covered by the three most recent studies: 100−760 Torr (this work), 7−15 Torr (Gilles et al.[20]), and 1 Torr (Bedjanian et al.[21]). The pressure-independence observed for k_1 in this work and the excellent agreement between the 100 Torr value of k_1 obtained in this work and that reported by Bedjanian et al. at 1 Torr support this assumption. Moreover, the good agreement between the branching ratio $((k_{1b} + k_{1c})/k_1)$ derived from the results of Gilles et al. at 7−15 Torr combined with this work at 100−760 Torr compared to that obtained by Bedjanian et al. at 1 Torr provides a further indication that k_1 is pressure independent.

The observed ratio of IO:BrO formed immediately following the reaction of O(^{3}P) with IBr (reaction 8) of 83%:17% is similar to the value reported by Laszlo et al.[19] of 74%:26%. As with the kinetic results, the difference between the studies can be attributed, at least in part, to the BrO cross sections used: Increase of the cross sections used by Laszlo et al. would reduce the measured [BrO] and bring the two results into closer agreement. The measurement of k_8 in terms of the branching ratio θ for the O(^{3}P) + IBr reaction reported here is to our knowledge the first determination of this rate coefficient.

The value obtained for the I + BrO reaction (k_{12}) at 298 K ($(1.3 \pm 1.2) \times 10^{-11}$ molecules^{-1} cm^3 s^{-1}) is in good agreement with other measurements of this rate coefficient of $(1.2 \pm 0.6) \times 10^{-11}$ (ref 19), $(1.45 \pm 0.20) \times 10^{-11}$ (ref 38), and $(1.9 \pm 1.1) \times 10^{-11}$ (ref 39) molecules^{-1} cm^3 s^{-1}. No other measurement of the temperature dependence of k_{12} has been reported.

5. Atmospheric Implications

The rate coefficient and products of the IO + BrO reaction have been shown to vary with temperature. Under conditions typical of the marine boundary layer/lower troposphere, the reaction proceeds with a rate coefficient of 8.5×10^{-11} molecules^{-1} cm^3 s^{-1}, and produces predominantly OIO + Br (65−93%), with minor channels which include one or more of I + Br + O_2, IBr + O_2, and/or OBrO + I. Occurrence of reaction 1 in the troposphere thus leads to the production of tropospheric OIO, the fate of which determines the role of this reaction. If OIO is photolabile, the formation of OIO from IO radicals and its subsequent photolysis lead to a null cycle with respect to ozone loss. Conversely, if, as has been suggested,[16] OIO is photostable, OIO may act as a hitherto unrecognized iodine reservoir in the troposphere and the role played by iodine species will depend on the homogeneous and heterogeneous reactivity of this species.

In the low stratosphere, typified by temperatures below 210 K, the IO + BrO reaction proceeds with a rate coefficient of the order of 2.5×10^{-10} molecules^{-1} cm^3 s^{-1}, and produces predominantly I + Br + O_2 (ca. 70%, assuming production of OBrO and $IBrO_2$ is negligible) with a minor channel forming OIO + Br (ca. 30%). The potential for the IO + BrO reaction to contribute to stratospheric ozone destruction is thus likely to be slightly greater than was assumed by Solomon et al.[8] However field measurements reporting generally low stratospheric IO concentrations, and the high yield of OClO measured for the IO + ClO reaction,[40,41] indicate that iodine chemistry, while it may contribute, is currently unlikely to be a major factor in stratospheric ozone depletion. No evidence for production of OBrO has been observed at 298 K in the course of this work, and OBrO production at lower temperatures is unlikely given the endothermicity of reaction 1d. The IO + BrO reaction is not the source of the atmospheric OBrO concentrations reported

by Renard et al.,[23] which are in any case unsupported by more recent observations.[6]

Acknowledgment. D.M.R. thanks the UK NERC for the award of an advanced fellowship. W.J.B. thanks the UK NERC for the award of a studentship. This work was part-funded by the EC Environment program under the project "Laboratory Experiments of Iodine Chemistry in the Stratosphere−LEXIS" (Project number ENV4-CT95-0013).

References and Notes

(1) Bloss, W. J.; Rowley, D. M.; Cox, R. A.; Jones, R. L. *J. Phys. Chem. A* **2001**, *105*, 7840.

(2) Harder, H.; Camy-Peyret, C.; Ferlemann, F.; Fitzednberger, R.; Hawat, T.; Osterkamp, H.; Schneider, M.; Perner, D.; Platt, U.; Vradelis, P.; Pfeilsticker, K. *Geophys. Res. Lett.* **1998**, *25*, 3843.

(3) Hegels, E.; Crutzen, P. J.; Klupfel, T.; Perner, D.; Burrows, J. P. *Geophys. Res. Lett.* **1998**, *25*, 3127.

(4) Pundt, I.; Pommereau, J. P.; Phillips, C.; Lateltin, E. *J. Atmos. Chem.* **1998**, *30*, 173.

(5) Wennberg, P. O.; Brault, J. W.; Hanisco, T. F.; Salawitch, R. J.; Mount, G. H. *J. Geophys. Res.* **1997**, *102*, 8887.

(6) Wittrock, F.; Müller, R.; Richter, A.; Bovensmann, H.; Burrows, J. P. *Geophys. Res. Lett.* **2000**, *27*, 1471.

(7) Platt, U. *Phys. Chem. Chem. Phys.* **1999**, *24*, 5409.

(8) Solomon, S.; Garcia. R. R.; Ravishankara, A. R. *J. Geophys. Res.* **1994**, *99*, 20491.

(9) Alicke, B.; Hebestreit, K.; Stutz, J.; Platt, U. *Nature* **1999**, *397*, 572.

(10) Fitzenberger, R.; Bosch, H.; Camy-Peyret, C.; Chipperfield, M. P.; Harder, H.; Platt, U.; Sinnhuber, B. M.; Wagner, T.; Pfeilsticker, K. *Geophys. Res. Lett.* **2000**, *27*, 2921.

(11) Carpenter, L. J.; Sturges, W. T.; Penkett, S. A.; Liss, P. S.; Alicke, B.; Hebestreit, K.; Platt, U. *J. Geophys. Res.* **1999**, *104*, 1679.

(12) Stutz, J.; Hebestreit, K.; Alicke, B.; Platt, U. *J. Atmos. Chem.* **1999**, *34*, 65.

(13) Rowley, D. M.; Harwood, M. H.; Freshwater, R. A.; Jones, R. L. *J. Phys. Chem.* **1996**, *100*, 3020.

(14) Poulet, G.; Biggs, P.; Burrows, J. P.; Cox, R. A.; Coutzen, P. J.; Hayman, G. D.; Jenkin, M. E.; LeBras, G.; Moortgat, G. K.; Platt, U.; Schindler, R. N. *Halogen Oxides: Radicals, Sources and Reservoirs in the Laboratory and in the Atmosphere*; Wayne, R. P., Ed.; European Commission: Brussels, 1995. Atmos. Environ. **1995**, *29*, 2675.

(15) Vaida, V.; Simon, J. D. *Science* **1995**, *268*, 1443.

(16) Cox, R. A.; Bloss, W. J.; Jones, R. L.; Rowley, D. M. *Geophys. Res. Lett.* **1999**, *26*, 1857.

(17) Misra, A.; Marshall, P. *J. Phys. Chem. A* **1998**, *102*, 9056.

(18) Guha, S.; Francisco, J. S. *J. Phys. Chem. A* **1997**, *101*, 5347.

(19) Laszlo, B.; Huie, R. E.; Kurylo, M. J. *J. Geophys. Res.* **1997**, *102*, 1523.

(20) Gilles, M. K.; Turnipseed, A. A.; Burkholder, J. B.; Ravishankara, A. R.; Solomon, S. *J. Phys. Chem. A* **1997**, *101*, 5526.

(21) Bedjanian, Y.; LeBras, G.; Poulet, G. *J. Phys. Chem. A* **1998**, *102*, 10510.

(22) Stutz, J.; Hebstreit, K.; Hoenninger, G.; Platt, U. *Geophys. Res. Abs.* **1999**, *1*, 520.

(23) Renard, J. B.; Pierre, M.; Robert, C. *J. Geophys. Res.* **1998**, *103*, 25383.

(24) Erle, F.; Platt, U.; Pfeilsticker, K. *Geophys. Res. Lett.* **2000**, *27*, 2217.

(25) Rattigan, O. V.; Jones, R. L.; Cox, R. A. *Chem. Phys. Lett.* **1994**, *230*, 121.

(26) Li, Z. *J. Phys. Chem. A* **1999**, *103*, 1206.

(27) Chipperfield, M. P.; Glassup, T.; Pundt, I.; Rattigan, O. V. *Geophys. Res. Lett.* **1998**, *25*, 3575.

(28) Harwood, M. H.; Rowley, D. M.; Jones, R. L.; Cox, R. A. *J. Phys. Chem. A* **1998**, *102*, 1790.

(29) Cole, L. G.; Elverum, G. W. *J. Chem. Phys.* **1952**, *20*, 1543.

(30) Wahner, A.; Ravishankara, A. R.; Sander, S. P.; Friedl, R. R. *Chem. Phys. Lett.* **1988**, *152*, 507.

(31) Atkinson, R.; Baulch, D. M.; Cox, R. A.; Hampson, R. F.; Kerr, J. A.; Troe, J. *J. Phys. Chem. Ref. Data* **1992**, *21*, 1125.

(32) Loewenstein, L. M.; Anderson, J. G. *J. Phys. Chem.* **1987**, *91*, 2993.

(33) Curtis, A. R.; Sweetenham, W. P. FACSIMILE, AERE Harwell Publication R 12805, Computer Science and Systems Division, Harwell Laboratory: Oxfordshire, U.K. 1987.

(34) Okafu, E. N.; Whittle, E. *Int. J. Chem. Kinet.* **1975**, *7*, 287.

(35) Miller, C. E.; Nickolaisen, S. L.; Francisco, J. S.; Sander, S. P. *J. Chem. Phys.* **1997**, *107*, 2300.

(36) Himmelmann, S. J.; Orphal, J.; Bovensmann, H.; Richter, A.; Ladstätter-Weissenmayer, A.; Burrows, J. P. *Chem. Phys. Lett.* **1996**, *251*, 330.

(37) Wilmouth, D. M.; Hanisco, T. F.; Donahue, N. M.; Anderson, J. G. *J. Phys. Chem. A* **1999**, *103*, 8935.

(38) Bedjanian, Y.; LeBras, G.; Poulet, G. *Chem. Phys. Lett.* **1997**, *266*, 233.

(39) Gilles, M. K.; Turnipseed, A. A.; Burkholder, J. B.; Ravishankara, A. R. *Chem. Phys. Lett.* **1997**, *272*, 75.

(40) Turnipseed, A. A.; Gilles, M. K.; Burkholder, J. B.; Ravishankara, A. R. *J. Phys. Chem. A* **1997**, *101*, 5517.

(41) Bedjanian, Y.; LeBras, G.; Poulet, G. *J. Phys. Chem. A.* **1997**, *101*, 4088.

(42) DeMore, W. B.; Sander, S. P.; Golden, D. M.; Hampson, R. F.; Kurylo, M. J.; Howard, C. J.; Ravishankara, A. R.; Kolb, C. E.; Molina, M. J. Chemical Kinetics and Photochemical Data for use in Stratospheric Modelling. Evaluation No. 12; JPL Publication 97-4; Jet Propulsion Laboratory: Pasadena, CA, 1997.

(43) Afeefy, H. Y.; Liebman, J. F.; Stein, S. E. Neutral Thermochemical Data. In *NIST Chemistry WebBook*; NIST Standard Reference Database Number 69; Mallard, W. G., Linstrom, P. J., Eds.; National Institute of Standards and Technology: Gaithersburg, MD, November 1998.

(44) Dolson, D. A.; Leone, S. R. *J. Chem. Phys.* **1982**, *77*, 4009.

(45) Haugan, H. K.; Weitz, E.; Leone, S. R. *Chem. Phys. Lett.* **1985**, *119*, 75.

(46) Burkholder, J. B. *Int. J. Chem. Kinet.* **1998**, *30*, 571.

(47) Jenkin, M. E.; Cox, R. A.; Mellouki, G.; LeBras, G.; Poulet, G. *J. Phys. Chem.* **1990**, *94*, 2927.

(48) Sander, S. P.; Watson, R. T. *J. Phys. Chem.* **1981**, *85*, 4000.